Modeling and Characterization of Soft Magnetic Film Actuated 2-D Scanners

Serhan O. Isikman, *Student Member, IEEE*, Olgaç Ergeneman, *Student Member, IEEE*, Arda D. Yalcinkaya, *Member, IEEE*, and Hakan Urey, *Member, IEEE*

***Abstract*—Magnetic behavior of polymer-based scanners is studied in detail with emphasis on a new magnetic actuator model and dc deflection experiments. A 30-μm-thick permalloy sheet is plated on a polymer cantilever scanner and actuated using an external coil. Mechanical and magnetic modeling of the device and experimental results are presented. Shape anisotropy of the thin, soft magnetic film is explored for push and pull operation in different configurations. A new magnetic actuator model is developed based on the distributed point-by-point calculation of the magnetostatic moments and forces across the film surface. This effort helps one to obtain generic equations for magnetic force and torque without limiting the use of the model to the case where magnetic material is assumed to be fully saturated. Two-dimensional (2-D) scanning utilizing the orthogonal modes of the scanner, using only one actuation coil is presented.**

***Index Terms*—Magnetic actuators, magnetic torque, optical scanning, permalloy, scanner.**

I. Introduction

MAGNETIC actuators have been used in different areas such as optical communications, display and imaging applications [1]–[7], biomedical applications, microfluidics [8], and relay switching [9]. Using magnetic actuators, relatively large forces can be obtained over large distances. They can make use of the Lorentz force [10], [11], [17], magnetostatic force with moving permanent magnets, or magnetic anisotropy torque with high-permeability thin films [4], [7], [11], [12], [16].

As illustrated in Fig. 1, the system described in this paper consists of a mirror suspended by a polymer cantilever beam, a permalloy sheet plated on the mirror, and an external coil to generate the driving magnetic field for dc and ac actuation. For the type of actuators studied in this paper, the simple linear magnetic circuit model studied in [15] fails, as most of the flux path is through the air. Furthermore, the saturated constant flux assumption cannot be used either [4], [5]. For a more accurate model, distributed magnetic moments and forces need to be computed using a nonlinear BH model for the magnetic film.

Manuscript received August 9, 2006; revised January 29, 2007. This work was supported in part by Koç University-Migros Joint Program (KUMPEM) and in part by two Scientific and Technological Research Council of Turkey (TÜBİTAK) under Project MİSAG-280-2004 and Project 104M161.

S. O. Isikman and H. Urey are with Koç University, Istanbul TR-34450, Turkey (e-mail: hurey@ku.edu.tr).

O. Ergeneman was with Koç University, Istanbul TR-34450, Turkey. He is now with Institute of Robotics and Intelligent Systems, ETH, Zurich, CH-8092, Switzerland.

A. D. Yalcinkaya was with Koç University, Istanbul TR-34450, Turkey. He is now with the Departmnet of Electrical and Electronics Engineering, Bogazici University, Istanbul TR-34342, Turkey.

Digital Object Identifier 10.1109/JSTQE.2007.893081

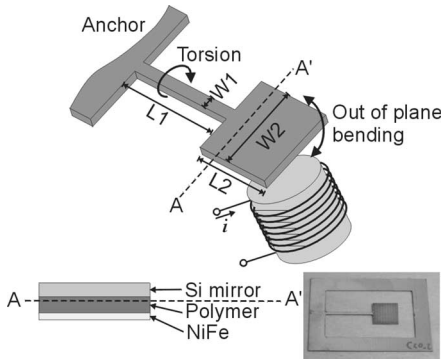

Fig. 1. Schematic (top) and photo (lower right) of the electrocoil-actuated scanner. The system consists of a narrow cantilever beam supporting a rectangular mirror and an electromagnet for actuation. Cross section between AA′ line is shown indicating the materials used in the structure. Torsional rotation and out-of-plane bending mode motion directions are marked with arrows.

Important contributions and novelties introduced by this study are: 1) demonstration of push or pull actuation by utilizing the shape anisotropy of the high-permeability magnetic films; 2) description of a method for magnetic force and torque calculation valid in nonuniform magnetic fields and both in saturated and unsaturated magnetic materials; 3) experimental validation of the dynamic resonant actuation using composite polymer material as the structural layer and electrodeposited magnetic films; and 4) two-dimensional (2-D) scanning using a single external actuation coil suitable for certain imaging and display applications. Millimeter-sized polymer devices are used in this study but the results are applicable to silicon microactuators as well.

This paper is organized as follows. Section II gives the details of the device operation. Mechanical structure of the device, design issues, and applied magnetic actuation scheme are addressed. Section III describes the 2-D imaging application of the device where a single electrocoil is used for actuation in two axes. Section IV states conclusions and a summary of the future work.

II. Device Operation

A. Structure of the Scanner

A schematic diagram of the scanner system studied in this paper is shown in Fig. 1. The device consists of a narrow cantilever beam supporting a rectangular mirror and an electromagnet for actuation. Polymer is used as the structural material because of its simple fabrication steps and mechanical properties. Permalloy is electroplated on the rectangular mirror part on one side and a 300-μm-thick silicon die with evaporated aluminum is

TABLE I
SCANNER DIMENSIONS AND MATERIAL PROPERTIES

Parameter	Symbol	Value
Width of the suspension	W_1	1 mm
Length of the suspension	L_1	15 mm
Width of the mirror	W_2	8 mm
Length of the mirror	L_2	8 mm
Polymer composite thickness	t_1	0.2 mm
Polymer composite Young's Modulus	E	52 GPa
Polymer composite density	ρ	4100 kg/m^3
Permalloy thickness	t_2	30 μm
Si die thickness	t	0.3 mm
Si Young's Modulus	E	1.63 10^9 Pa

attached as a mirror on the other side. The thickness of silicon layer is sufficient to prevent dynamic mirror deformation, which should be less than one-tenth of the wavelength used in the system for diffraction-limited optical performance. The cantilever beam is anchored at its narrow end. Table I shows the material properties and dimensions of the supporting beam and mirror.

B. Dynamic Mechanical Operation

The scanner works on the principle that the mirror deflects the light beam falling on itself to form a scan line on a desired target. Cantilever-type scanner is tailored to have its fundamental resonance mode in the out-of-plane direction. The first resonance mode frequency of the cantilever-type scanner is calculated as [13]

$$\omega_0 = \sqrt{\frac{k_S - k_F}{J}} \tag{1}$$

where k_S is the stiffness of the suspension calculated through the Young's modulus of the polymer and the geometry of the spring, k_F is the spring softening term that is dependent on the actuation power, and J is the effective mass moment of inertia. Essentially, one can design the resonance frequency by changing the suspension and the mirror dimensions. For the scanner geometries given in Table I, the fundamental cantilever bending mode occurs at 56.5 Hz. This mode is used in scan operations for barcode readers, where the scanning mirror is moving out-of-plane. The other useful motion is excited at the third mode at 340 Hz, where the torsion about the suspension is observed. This mode is utilized to form a scan line orthogonal to the one created by the fundamental mode for 2-D raster-like scanning. It is worth noting that the scanner works as a coupled multi-bandpass filter, where modes are well separated due to the high quality-factor of each mode [11].

Electromechanical transfer function of the device is extracted by the dynamic deflection measurements using a laser Doppler vibrometer (LDV). Fig. 2(a) shows the peak-to-peak optical-scan-angle in the fundamental mode as a function of frequency when the RMS electrocoil drive current is 28 mA. Using an 8-mm scanner, the peak-to-peak optical-scan-angle and mirror-size product (θD-product) of 144 deg·mm was obtained with a power consumption of 168 mW for slow-scan axis at 56.5 Hz.

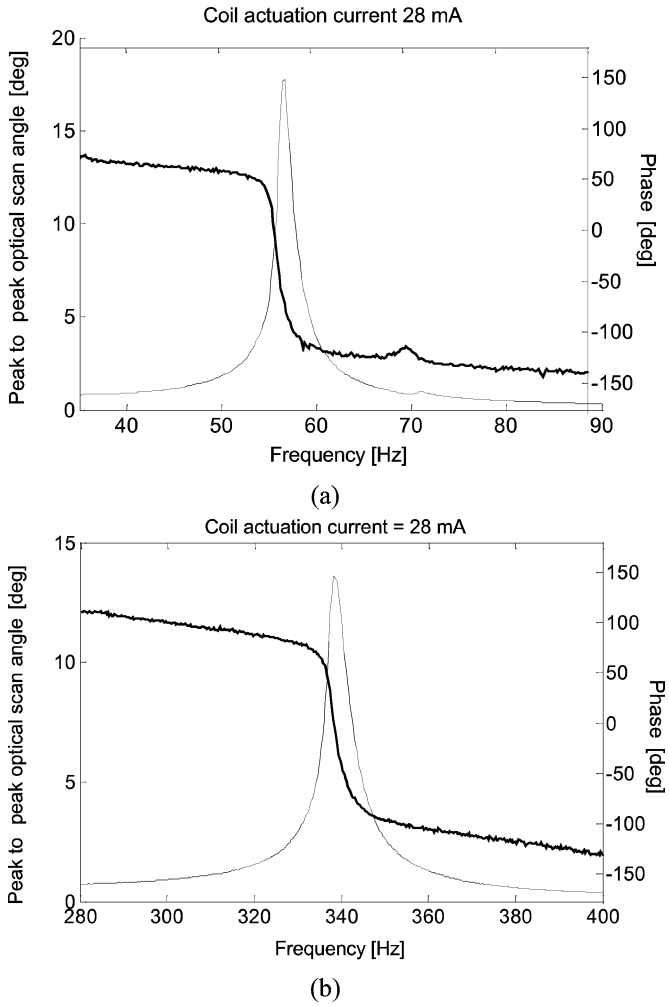

Fig. 2. Resonance characteristics of the polymer scanner. (a) Fundamental (out-of-plane bending) mode. (b) Torsion mode. The total optical scan angles plotted in both graphs are twice the total mechanical scan angles.

This θD-product corresponds to about 2800 resolvable spots in an imaging system assuming adjacent spots overlap at full-width at half-maximum intensity [14]. Similarly, by consuming the same amount of power, fast-scan axis at 340 Hz can supply a θD-product of 101 deg·mm (or about 2000 resolvable spots). Fig. 2(b) shows the peak-to-peak optical-scan-angle in the torsion mode. The mechanical quality factors of these motions, measured at atmospheric pressure, are 40 (out-of-plane mode) and 87 (torsion mode).

As a result of spring softening effect, modeled with k_F term in (7), the resonance frequency tends to get lower in a linear fashion, as shown in Fig. 3. In this graph, the experimental data are collected by recording the peak displacements appearing in resonance for varying actuation levels. Effectively, by changing the electrocoil current in the range 2–16 mA one can tune the resonance frequency by as much as 2%.

As can be seen in Fig. 3, the cantilever tip displacement is reduced as the electrocoil current is increased. This stems from the complex character of the mechanical torque, which is produced

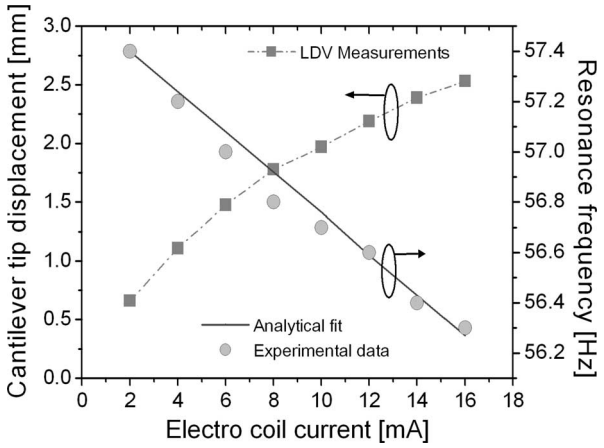

Fig. 3. Spring softening effect and the effect of varying actuation force on the cantilever displacement.

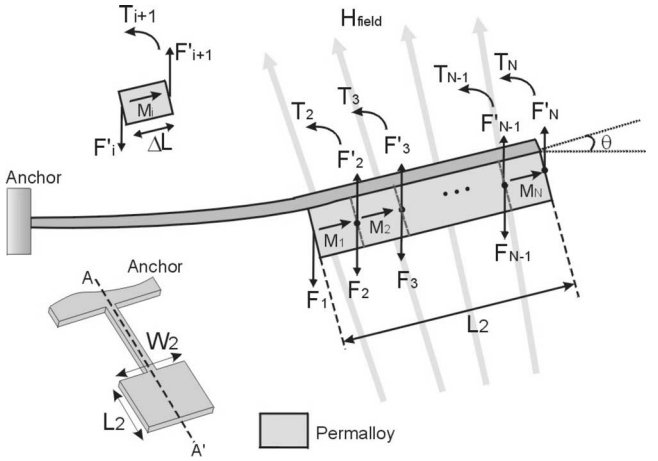

Fig. 4. Moments $(T_2, T_3, \ldots, T_N)$ and forces $(F_1, F_{2'}, \ldots, F_{N-1}, F_{N'})$ acting on the magnetic material volume elements. The inset shows one such volume element (due to rectangular shape of the coil, an average field value assumed over the W_2 geometry results in approximately the same net force and net torque with the case where W_2 is divided into $(N-1)$ segments.).

by the product of the magnetic field and the magnetization. These effects will be described in detail in the next section.

III. Magnetic Actuator Model

The magnetic properties of a sample depend on the direction in which they are measured. This is a result of the magnetic anisotropy that becomes an important factor in determining the suitability of the magnetic material in a particular application. The directions of the easy and hard axes are determined by the magnetic anisotropy of a sample. There are different sources of magnetic anisotropy such as crystalline anisotropy, induced anisotropy, stress anisotropy, and shape anisotropy [4]. In an ideal hard magnetic material, the magnetization vector does not change in magnitude, and it does not rotate away from the easy axis. But in soft magnetic materials, the magnetization vector can rotate away from its initial preferred position. The rotation angle of the magnetization vector is determined by the magnetic anisotropy energy, which depends on the material properties and sample geometry.

We reconsider the structure illustrated in Fig. 1 where the 30-μm-thick permalloy is plated as a thin film across the 8 mm $\times$ 8 mm mirror piece. The shape anisotropy is assumed to be dominant due to large length-to-thickness ratio for the magnetic material; thus, the magnetization vector remains parallel to the surface of the mirror plate [2]. The magnetic field (H_{field}) and the magnetization across the material created by the electromagnet is not uniform across the mirror. In all the calculations, the mirror plate is assumed rigid, and the bending takes place in the cantilever beam.

The new magnetic model for force and torque calculation is illustrated in Fig. 4 across the cross-section AA'. The magnetic material is divided into volumetric elements with uniform thickness (t_2) and width (W_2) where each element has a respective magnetization direction with positive and negative poles at each end. The array model developed here can be considered as an extension of the single magnetic element model presented in [5]. The distributed forces and moments due to varying magnetic field on the magnetic material are formed, as shown in Fig. 4. The distributed forces on each small section are multiplied by the corresponding distances to the anchor to obtain the corresponding torque. Finally, contribution from every section is added to find the total net force and the torque. The total tip deflection and rotation due to the net force and torque applied at the tip of the cantilever are then calculated using superposition.

The permalloy M–H relationship is modeled as linear until the field is sufficiently large to saturate the material. The saturation magnetization M_s is assumed as 0.75 T, and the relative permeability is used as a fit parameter for the experimental data. The model is valid in nonuniform external fields for both saturated and unsaturated magnetic material cases but does not include hysteresis effects.

The permalloy film surface is divided into $(N-1)$ equal-sized volume elements with uniform thickness (t_0), width (W_2), and length ΔL where $L_2 = (N-1)\Delta L$. The magnetic field for each element is different, i.e., the left and right sides of the ith volume element experiences fields H_i and H_{i+1}, respectively. This will lead us to the following force equations:

$$\begin{aligned} F_1 &= M_1 W_2 t_2 H_1 \\ F_2' &= M_1 W_2 t_2 H_2 \\ F_2 &= M_2 W_2 t_2 H_2 \\ F_{N-1} &= M_{N-1} W_2 t_2 H_{N-1} \\ F_N' &= M_N W_2 t_2 H_N \end{aligned} \tag{2}$$

Assuming the mirror is rigid, the resulting net force at the tip of the cantilever is given as

$$F_{\text{NET}} = \sum_{i=1}^{N-1} F_i - F_{i+1}' \tag{3}$$

If the magnetization is uniform across the material, the net force simplifies to $F_{\text{NET}} = F_1 - F_N'$ that is consistent with [5] when the number of pieces is one (i.e., $N - 1 = 1$).

Likewise, the torque (or moment) associated with each magnetic piece with respect to the tip of the cantilever can be calculated as

$$\begin{aligned} T_2 &= (F_2' - F_2)\Delta L \cos\theta \\ T_3 &= (F_3' - F_3)2\Delta L \cos\theta \\ T_4 &= (F_4' - F_4)3\Delta L \cos\theta \\ &\vdots \\ T_{N-1} &= (F_{N-1}' - F_{N-1})(N-2)\Delta L \cos\theta \\ T_N &= F_N(N-1)\Delta L \cos\theta \end{aligned} \tag{4}$$

where θ is the total angular deflection of the scanner tip due to the net force and torque. Therefore, the net torque is

$$T_{\mathrm{NET}} = \sum_{i=2}^{N} T_i \tag{5}$$

which is consistent with [5] when the number of pieces is one (i.e., $N-1=1$). The mechanical deflection can therefore be found when the net force is known. The mechanical restoring force is given by

$$F_{\mathrm{mech}} = -k\delta_{\mathrm{force}} \tag{6}$$

where k is the linear spring constant of the flexure in the bending mode and δ_{force} is the static mechanical deflection of the tip of the scanner due to magnetic force. In the calculation of k, effective Young's modulus and effective density of the seed layer for electroplating are taken into account as well. In equilibrium, the total net force is equal to zero, $F_{\mathrm{field}} + F_{\mathrm{mech}} = 0$. Thus, δ_{force} is given by

$$\delta_{\mathrm{force}} = \frac{F_{\mathrm{field}}}{k}. \tag{7}$$

The mechanical deflection angle and the related mechanical deflection can therefore be found if the net torque is known. The mechanical restoring torque, due to the suspension of the structure, T_{mech} is given by

$$T_{\mathrm{mech}} = -k_\phi \phi \tag{8}$$

where k_ϕ is the angular spring constant of the flexure in the bending mode and ϕ is the static angular deflection of the tip of the scanner due to magnetic torque. In equilibrium, total net torque is equal to zero $T_{\mathrm{field}} + T_{\mathrm{mech}} = 0$; thus, ϕ can be found by

$$\phi = \frac{T_{\mathrm{field}}}{k_\phi}. \tag{9}$$

The tip deflection of a cantilever due to a moment applied at the tip is given by [18]

$$\delta_{\mathrm{torque}} = \frac{L_1}{2}\phi. \tag{10}$$

The total tip deflection can be found by combining (7) and (10)

$$\delta_{\mathrm{total}} = \delta_{\mathrm{force}} + \delta_{\mathrm{torque}} \tag{11}$$

Fig. 5 shows the experimental and finite element method (FEM) simulation results of the perpendicular and radial fields (B_z and B_r) of the applied magnetic flux density across the magnetic film. FEM simulations are performed on an axially symmetrical coil for more accurate 2-D magnetic modeling. This results in a negligible difference between the FEM simulations and experimental results around the edges of the coil. The experimental data are obtained by first placing the scanner at the center of the coil, and then moving it along the horizontal axis. H_z and H_r values obtained from FEM analysis are used in the torque calculations. In order to account for the change in H_z and H_r relative to the radial distance, the total torque is computed as a summation of distributed torque that is proportional to $H_r H_z$ product when the magnetic material is not saturated and is proportional to $M_s H_z$ product for the parts of the material that are saturated [4].

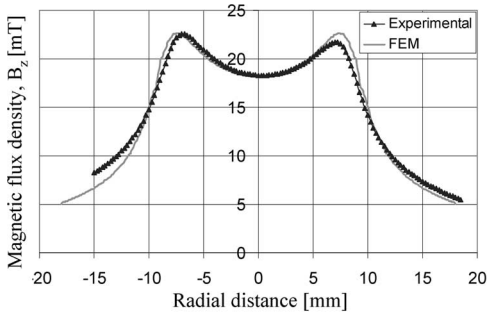

(a)

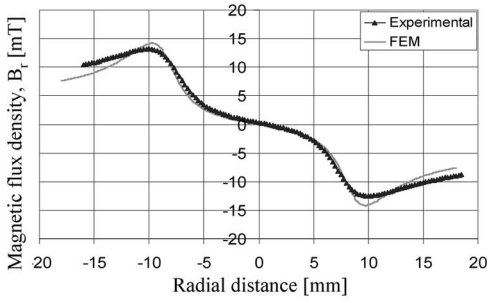

(b)

Fig. 5. Experimental and FEM simulation results for 500-mA dc coil current. (a) Vertical component B_z and (b) radial component B_r of the magnetic flux density different radial distances between the centers of the scan mirror and the coil.

The model presented could also be straightforwardly implemented for the torsion mode of the scanner. However, the torque on both sides of the beam would cancel each other if coil is centered with respect to the scanner. Therefore, in order to operate the device in dc torsion mode, a different coil placement would be required to increase twisting moment. Nevertheless, for resonant actuation, asymmetries in the structure would be enough to start the vibrations and lead to large deflections of the actuator.

Soft magnetic materials are known to be attracted toward magnets or electromagnets (e.g., a scissor is always attracted toward a magnet). However, as illustrated in Fig. 6, in thin magnetic films, the mechanical deflection can be bidirectional. Due to the high shape anisotropy, the magnetization does not rotate and remains an in-plane one, and the entire structure experiences a torque, which can be bidirectional. The direction of the torque is determined by the direction of the magnetic flux

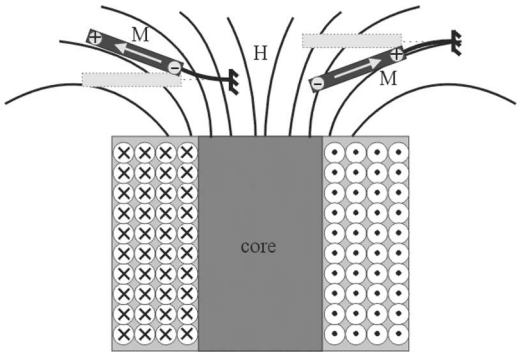

Fig. 6. Magnetization vector tries to align with the magnetic field lines. On the left of the electromagnet the magnetization is leftward so the scanner deflects upward (push) and on the right the magnetization is rightward so the scanner deflects downward (pull).

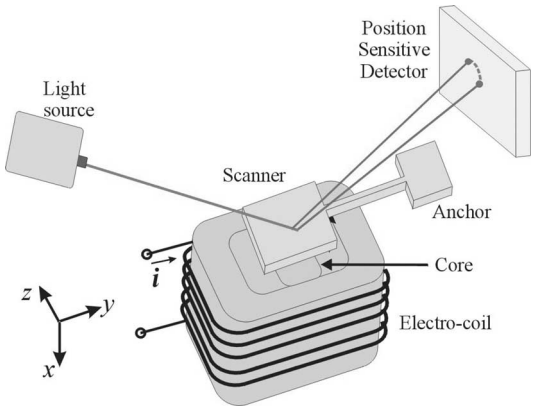

Fig. 8. Illustration of the static deflection measurement setup. Coil dimensions for x, y, z : 61.5 mm $\times$ 61.5 mm $\times$ 60 mm, respectively. Ferromagnetic core dimensions for x, y, z : 29 mm $\times$ 16 mm $\times$ 62 mm, respectively.

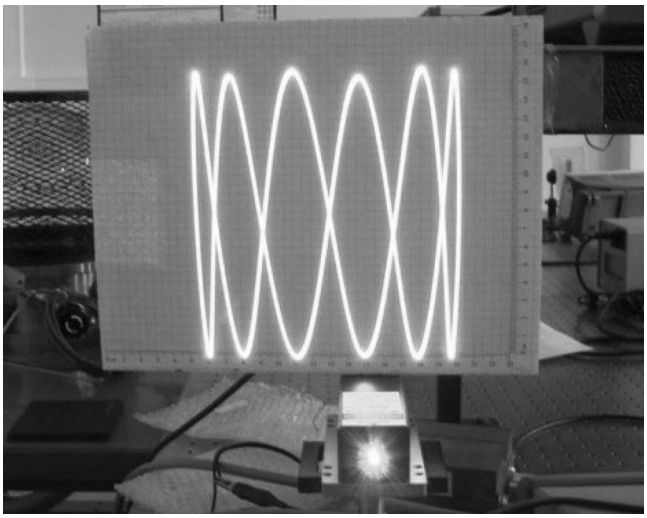

Fig. 7. 2-D image formed by the scanner.

lines and the anchor point of the structure. Unlike permanent magnets, changing the coil current direction does not change the direction of the actuation. For the scissor example, however, the magnetization does not have a strong preferred direction and rotates to align itself with the external field resulting in an attractive force. The translational magnetic force toward the magnet is then produced by the large field gradient to maximize the magnetostatic energy [5].

Simultaneous excitation of the bending and torsion modes (modes 1 and 3) yields a 2-D raster-like resonant motion when the structure is energized with proper signals. More specifically, when the electrocoil is driven by the sum of two sinusoids at the frequencies of the out-of-plane bending and the torsion modes, a force proportional to i_{total} will be exerted [11]

$$i_{\text{total}} = i_1 \sin(\omega_1 t) + i_3 \sin(\omega_3 t) \tag{12}$$

where ω_1 and ω_2 are the resonance frequencies of the out-of-plane bending and torsion modes of the scanner. A 2-D scan pattern, shown in Fig. 7, is created by using only one actuation coil driven with a current signal as in (12). The scanner is kept in two-mode coupled resonance. Moderately high mechanical quality factors of the modes separate the motions in two axis, acting as a bandpass filter with multipass bands, and each resonance mode yields in a scan line orthogonal to the other one. A similar actuation principle was previously applied to Lorentz force electromagnetic microelectromechanical system (MEMS) scanners [11].

IV. Magnetic Actuator Characterization and Model Validation

The static deflection measurement setup is used to obtain the experimental deflections. The illustration of the static deflection measurement setup is shown in Fig. 8. A laser beam illuminated a tiny spot on the scan mirror, and the reflected light is incident on a position sensitive detector (PSD). The device under test is actuated by the help of an electromagnet. When a dc current is applied to the electromagnet, the device deflects and changes the position of the laser spot of the reflected light on the PSD. The PSD measures the centroid of the laser spot; one has to make sure that the out-of-plane deflection and the rotation of the scanner are decoupled during this measurement. The static deflection measurement setup has submicrometer sensitivity, and it requires reflective surfaces for measurements.

Experimental results on tip deflection versus applied drive currents at low and high magnetic fields are given in Fig. 9(a) and (b), respectively. Theoretical calculations shown in these plots assume the relative permeability of the magnetic material is 150 and M_s is 0.75 T. As seen in the Section II, the magnetic force and torque on each volume element are proportional to the product of H_z and M and M increases with H_r, as defined by the M–H loop of the magnetic material, until the volume element is saturated. For low-current values, the element is not saturated, and the torque increases with the square of the applied current. For large current values, the material is saturated (i.e., $M = M_s$) and the torque increases linearly with current. Note that the position of the transition from quadratic to linear relationship is determined not only by the applied current, but also with the relative position of the electromagnet owing to the nonuniform magnetic field. For small values of $y(|y| < 4.5)$, as shown in

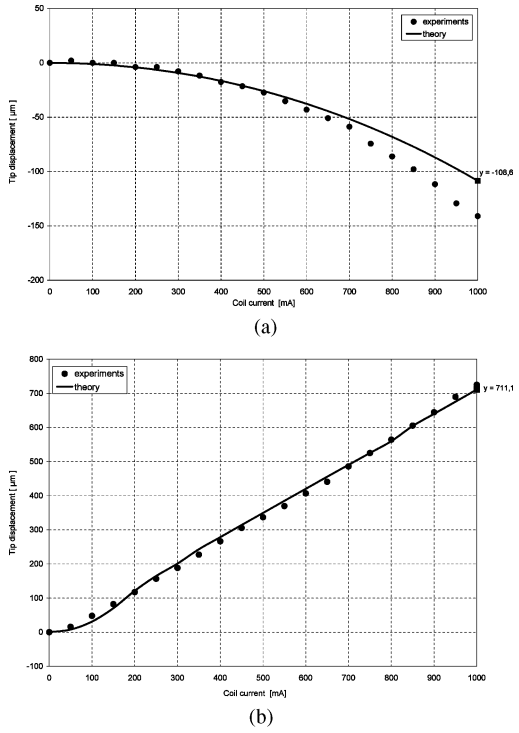

Fig. 9. Scanner tip deflection at a nominal scanner-coil distance of $z = +1.5$ mm as a function of the applied current. (a) scanner is placed at $y = -1$ mm radial distance, (b) scanner is placed at $y = +10$ mm radial distance.

Fig. 9(a), the radial component of the magnetic field is weak, and it takes large currents to saturate the magnetic material and most of the volume elements are not saturated. For large values of y (e.g., $|y| > 4.5$ mm), as shown in Fig. 9(b), the magnetic field lines that interact with the scanner are bent away from the vertical direction, and H_r is larger than H_z. Around these locations, most of the volume elements are saturated at much lower currents and the torque–current relationship is mostly linear. The theoretical calculations based on the model developed in the previous section and the experimental measurements agree quite well.

Fig. 10 shows the theoretical and the experimental tip deflections at 1000-mA dc current as a function of the radial (y) distance. Positive radial distance is toward the side where the mirror suspension is anchored. The positive and negative tip deflections correspond to the pull and push regions of the actuator, respectively, and there is a point near $y = +0.5$ mm where the forces and moments on either side of the structure cancel each other due to the opposite magnetic moment directions. As the electromagnet is moved in the $+y$ direction, the magnetic force gets larger toward the tip of the cantilever scanner, thereby producing a larger torque compared to that produced when moving in the other direction. Had the mirror and the film been treated as a point object, the deflection would be radially symmetric. Although push and pull actuation is possible with single electrocoil, force is still unidirectional with its direction dependent on the relative position of the scanner with respect to coil. Hence, manual adjustment of the anchor point is required for choosing between push or pull actuation. However, by magnetizing the permalloy layer in a fixed direction using an external permanent magnet, bidirectional force generation could be achieved by changing the direction of the coil current.

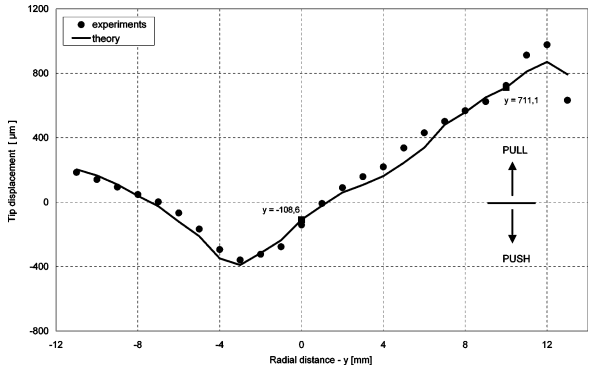

Fig. 10. Tip deflection as a function of the radial (y) distance at 1000-mA coil current. The scanner is placed at the center of the electromagnet and 1.5 mm away from its top surface. It is moved in the positive and negative directions along the y axis without changing the x and z displacement.

V. Conclusion

In this paper, modeling, design, and characterization of polymer-based electromagnetic scanners are described. It is experimentally shown that the present device is capable of being used as a 2-D imaging device by using a simple one-coil driving scheme. Conformity between the magnetic simulations/calculations and experimental characterizations is successfully demonstrated to show push or pull actuation stemming from the shape anisotropy of the magnetic film. A new model is developed and validated with experiments for magnetic actuators employing thin magnetic films. The model is valid in nonuniform fields for both saturated and unsaturated magnetic material cases but does not include hysteresis effects. Device operation in a nonuniform field is explained in theory and supported by the mechanical displacement testing in relation to the applied magnetic field. It is experimentally proved that use of polymers for 1-D and 2-D scanning applications can yield in high performance as well as low fabrication costs and actuation power levels. Magnetic actuator modeling results are also applicable to smaller MEMS devices. Additionally, using this model, it can also be shown that the angular displacement of the scanner is independent of the scaling of the system dimensions as long as current is kept constant. If s is a scaling parameter that multiplies all the dimensions of the actuation coil and the scanner, the resonant frequency is inversely proportional to s while the scan angle is independent of s. Hence, the product of mirror size, scan angle, and frequency, which is an important figure of merit for assessing the scanner resolution and speed performance, remains constant and the actuator lends itself well to miniaturization. Hence, miniaturization of the whole system does not affect the scanning performance. The device can be fabricated using MEMS technology with integrated actuation coil using standard micromachining techniques.

ACKNOWLEDGMENT

The Authors would like to thank Aselsan A. Ş., Ankara, Turkey, for their help in fabrication of some of the prototypes.

REFERENCES

[1] G. F. Marshall, Ed., *Optical Scanning*. New York: Dekker, 1991.
[2] O. Ergeneman, A. D. Yalcinkaya, and H. Urey, "Polymer based electromagnetic scanners for barcode applications," in *Proc. 16th Micromech. Eur. (MME) Workshop*, 2005, pp. 370–373.
[3] B. Wagner, M. Kreutzer, and W. Benecke, "Electromagnetic micro actuators with multiple degrees of freedom," in *Proc. 6th Int. Conf. Solid-State Sens. Actuators*, San Francisco, CA, 1991, pp. 614–617.
[4] J. Judy and R. S. Muller, "Magnetically actuated, addressable microstructures," *IEEE/ASME J. Microelectromech. Syst.*, vol. 6, no. 3, pp. 249–256, Sep. 1997.
[5] C. Liu and Y. W. Yi, "Micromachined magnetic actuators using electroplated permalloy," *IEEE Trans. Magn.*, vol. 35, no. 3, pp. 1976–1985, May 1999.
[6] D. Ciudad, C. Aroca, M. C. Sanchez, E. Lopez, and P. Sanchez, "Modeling and fabrication of a MEMS magnetic sensor," *Sens. Actuators A*, to be published.
[7] A. D. Yalcinkaya, O. Ergeneman, and H. Urey, "Polymer magnetic scanners for bardcode applications," *Sens. Actuators A, Phys.*, vol. 135, no. 1, pp. 236–243, 2007.
[8] C. Liu, T. Tsao, G. Lee, J. T. S. Leu, Y. W. Yi, Y. Tai, and C. Ho, "Out-of-plane magnetic actuators with electroplated permalloy for fluid dynamics control," *Sens. Actuators A*, vol. 78, pp. 190–197, 1999.
[9] M. Ruan, J. Shen, and C.B. Wheeler, "Latching micro magnetic relays," *IEEE/ASME J. Microelectromech. Syst.*, vol. 10, no. 4, pp. 511–517, Dec. 2001.
[10] R. B. Sprague, T. Montague, and D. Brown, "Bi-axial magnetic drive for scanned beam display mirrors," *Proc. SPIE, MOEMS Display Imag. Syst. III*, vol. 5721, pp. 1–13, 2005.
[11] A. D. Yalcinkaya, H. Urey, T. Montague, D. Brown, and R. Sprague, "Two-axis electromagnetic microscanner for high resolution displays," *IEEE/ASME J. Microelectromech. Syst.*, vol. 15, no. 4, pp. 786–794, Aug. 2006.
[12] J. W. Judy, R. S. Muller, and H. H. Zappe, "Magnetic micro actuation of polysilicon flexure structures," *J. Microelectromech. Syst.*, vol. 4, no. 4, pp. 162–169, 1995.
[13] H. Urey, C. Kan, and W. Davis, "Vibration mode frequency formulae for micromechanical scanners," *J. Micromech. Microeng.*, vol. 15, pp. 1713–1721, 2005.
[14] H. Urey, "Retinal scanning displays," in *Encyclopedia of Optical Engineering*, vol. 3, R. Driggers, Ed. New York: Dekker, 2003, pp. 2445–2457.
[15] Y. Nemirovsky, I. Zelniker, O. Degani, and G. Sarusi, "A methodology and model for the pull-in parameters of magnetostatic actuators," *J. Microelectromech. Syst.*, pp. 1253–1264, vol. 14, no. 6, Dec. 2005.
[16] D. C. Jiles and C. C. H. Lo, "The role of new materials in the development of magnetic sensors and actuators," *Sens. Actuators A*, vol. 106, pp. 3–7, 2003.
[17] Y. Haga, W. Makishi, K. Iwami, K. Totsu, K. Nakamura, and M. Esashi, "Dynamic Braille display using SMA coil actuator and magnetic latch," *Sens. Actuators A*, vol. 119, pp. 316–322, 2005.
[18] W. C. Young and R.G. Budynas, *Roark's Formulas for Stress and Strain*, 7th ed. New York: McGraw-Hill, 2002.

Serhan Isikman (S'02) was born in Ankara, Turkey, in 1983. He received the B.S. degree in electrical and electronics engineering (with merit-based scholarship from Koç Vakfi) from Koç University, Istanbul, Turkey, in 2006, where he is currently working toward the M.Sc. degree.

Mr. Işikman is a recipient of the graduate study scholarship from the Scientific and Technological Research Council of Turkey (TUBITAK) during 2006–2008.

Olgaç Ergeneman (S'04) was born in Ankara, Turkey, in 1981. He received the B.S. degree in electrical and electronics engineering from Middle-East Technical University, Ankara, in 2003, and the M.Sc. degree in electrical engineering from Koç University, Istanbul, Turkey. Currently, he is working toward the Ph.D. degree at the Institute of Robotics and Intelligent Systems, ETH, Zurich, Switzerland.

Mr. Ergeneman is a student member of the International Society for Optical Engineers (SPIE).

Arda D. Yalcinkaya (S'97–A'98–M'07) received the B.S. degree from Istanbul Technical University, Istanbul, Turkey, and the M.Sc. and Ph.D. degrees from Danmarks Tekniske Universitet (DTU), Mikroelektronik Centret, Lynby, Denmark, all in electrical engineering in 1997, 1999, and 2003, respectively.

During 1999–2000, he was a Research and Development Engineer at Aselsan Microelectronics, Ankara, Turkey. He was a Visiting Reseacher at Interuniversity Microelectronic Center (IMEC), Leuven, Belgium, and Centro Nacionale de Microelectronica (CNM), Barcelona, Spain, in 2000 and 2003. During 2003–2006, he was a Postdoctoral Research Associate at Koç University, Istanbul. During that period he served as a Consultant to Microvision Inc., Seattle, WA. Currently, he is an Assistant Professor of electrical engineering at Bogazici University, Istanbul. His current research interests include design, fabrication, and characterization of microelectromechanical systems (MEMS), CMOS-MEMS integration, nanotechnology, and design of analog application-specified integrated circuits (ASICs). He received the Sabanci Foundation (VAKSA) Turkish Education Foundation (TEV) scholarships during his studies.

Hakan Urey (S'91–M'96) received the B.S. degree from Middle East Technical University, Ankara, Turkey, in 1992, and the M.S. and Ph.D. degrees from Georgia Institute of Technology, Atlanta, in 1996 and in 1997, all in electrical engineering.

He is currently an Assistant Professor of Electrical Engineering at Koç University, Istanbul, Turkey. He was a Graduate Research Assistant with Bilkent University, Ankara, and Georgia Tech Research Institute, Atlanta, and was a Consultant with Call/Recall Inc., San Diego. He joined Microvision Inc., Seattle, WA, in 1998, and became the Principal System Engineer, and since 2002, has been a Consultant for the company. He has published more than 60 journal and conference papers, six edited books, two book chapters, and he is the holder of 12 issued and several pending patents. His current research interests include scanning systems, microoptics, optical microelectromechanical systems (MEMS), optical system design, and display and imaging systems.

Dr. Urey is a member of the International Society for Optical Engineers (SPIE), Optical Society of America (OSA), IEEE-Lasers and Electro-Optic Society (LEOS), and Vice-President of the Turkey chapter of IEEE-LEOS. He received the Werner Von Siemens Faculty Excellence Award in 2006.